

# On the natural variability of the pre-industrial European climate

Lennart Bengtsson · Kevin I. Hodges ·  
Erich Roeckner · Renate Brokopf

Received: 23 January 2006 / Accepted: 12 June 2006 / Published online: 14 July 2006  
© Springer-Verlag 2006

**Abstract** We suggest that climate variability in Europe for the “pre-industrial” period 1500–1900 is fundamentally a consequence of internal fluctuations of the climate system. This is because a model simulation, using fixed pre-industrial forcing, in several important aspects is consistent with recent observational reconstructions at high temporal resolution. This includes extreme warm and cold seasonal events as well as different measures of the decadal to multi-decadal variance. Significant trends of 50-year duration can be seen in the model simulation. While the global temperature is highly correlated with ENSO (El Niño–Southern Oscillation), European seasonal temperature is only weakly correlated with the global temperature broadly consistent with data from ERA-40 reanalyses. Seasonal temperature anomalies of the European land area are largely controlled by the position of the North Atlantic storm tracks. We believe the result is highly relevant for the interpretation of past observational records suggesting that the effect of external forcing appears to be of secondary importance. That variations in the solar irradiation could have been a credible cause of climate variations during the last centuries, as suggested in some previous studies, is presumably due to the fact that the models used in these studies may have underestimated the internal variability of the climate. The general interpretation from this study is

that the past climate is just one of many possible realizations and thus in many respects not reproducible in its time evolution with a general circulation model but only reproducible in a statistical sense.

## 1 Introduction

Commendable efforts to reconstruct the Earth’s climate over the last 1,000 years or so have been undertaken in recent years with the help of palaeo data (e.g. Jones and Mann 2004 and references therein). These reconstructions differ from each other but indicate generally lower temperatures than present and show variability on all resolvable time scales. Some reconstructions show a slowly decreasing temperature trend between the year 1000 and the end of the 19th century, thereafter a warming trend broadly in agreement with different climate simulations using observed greenhouse gases and selected aerosols. The warming trend becomes most pronounced during the last decades of the 20th century.

There have been several studies attempting to explain the climate fluctuations prior to the end of the 19th century. During this period the variations in the Green House Gases (GHG) were minor, so the main candidates for forcing proposed in these studies are solar variability and volcanic eruptions (e.g. Mann et al. 1999). The major volcanic records have been reconstructed, mainly with the help of ice core measurements (Robock and Free 1995, 1996 and Robertson et al. 2001), whilst, the Total Solar Irradiation (TSI) has been reconstructed with the help of sun spot

---

L. Bengtsson · K. I. Hodges  
Environmental Systems Science Centre, Harry Pitt Building,  
Whiteknights, P. O. Box 238, Reading RG6 6AL, UK

E. Roeckner · R. Brokopf · L. Bengtsson (✉)  
Max Planck Institute for Meteorology, Bundesstraße 53,  
20146 Hamburg, Germany  
e-mail: bengtsson@dkrz.de

observations, isotope measurements of Beryllium-10 ( $^{10}\text{Be}$ ) and Carbon-14 ( $^{14}\text{C}$ ) combined with hypotheses of solar variability (e.g. Lean et al. 1995; Solanki et al. 2004). However, recent observational studies suggest that the solar irradiation records previously published (Hoyt and Schatten 1993; Lean et al. 1995) indicate a too large variability of TSI (Wang et al. 2005). The latest available compilation of TSI from satellite based measurements, including three solar cycle maxima (Fröhlich 2004, 2006); show that the observed trend of TSI variability for 1978–2005 is not significantly different from zero. Furthermore, the relation between sun spots and TSI (C Fröhlich, personal communication, 2005) as well as between isotope measurements and TSI (B Heber, personal communication, 2005) needs to be further assessed before any reliable statement can be made about the longer term variability of TSI. The decadal to centennial variability of TSI is still, in all respects, an open issue. Consequently, model simulations using available records of anticipated solar forcing (e.g. Cubasch et al. 1997) may have to be reconsidered.

Many of the observed variations of the pre-industrial climate can also be associated with internal processes of the ocean/atmosphere/land system. We know, for example, that major climate anomalies on a global scale are related to El Niño/Southern Oscillation (ENSO) events. Similarly, the phase and amplitude of the large centres of actions in the atmosphere such as North Atlantic Oscillation (NAO) and Pacific North American (PNA) pattern have a major influence on the extratropical/tropical regional climate (e.g. Hurrell et al. 2003; Brönnimann et al. 2004).

In order to interpret past climate records, it is essential to gain a more in depth knowledge of the unforced variability. Needless to say, forcing from volcanic eruptions is likely to influence climate, but presumably only for short time periods of at most a few years. This does not include super eruptions or sequences of major eruptions over a longer period. However, such events are not likely to have occurred during the last 500 years. Changes in solar variability may also have influenced the climate, but so far no reliable observational data are available to support this. However, we would be inclined to suggest that if the long term simulated variability is less than the variability estimated from observations or proxy data, an additional external forcing on climate such as solar forcing is more likely to exist. Alternatively, if the simulated variability is in good agreement with the estimated variability from observational records a hypothetical external forcing is less credible unless supported by independent observations. It is therefore

of considerable interest to explore the natural climate variability using a state of the art coupled climate model.

The main objective in this study is to assess the typical pre-industrial internal variability of a high resolution, state-of-the-art, coupled model over a period of several hundred years. The comparison is limited to the time period 1500–1900, but some examples from the first part of the 20th century are used (as global seasonal data before 1900 are less reliable) in order to see the European climate in a global context. It has not been our aim to try to reproduce the European climate as it has evolved, as we do not think this is feasible for such a limited space and time scale, even if we had a complete knowledge of the external forcing (Boer and Yu 2003a, b). The dominant role of internal processes for the extra-tropical regional climate is further supported by a recent assessment of the Arctic climate in the 20th century (Johannessen et al. 2004; Bengtsson et al. 2004; J Overland, personal communication, 2005). See also Yoshimori et al. (2005).

It has been suggested that a detailed knowledge of the external forcing, would make it possible to reproduce climate variations as they have evolved over time, and some attempts to do so have been undertaken by, Cubasch and Voss (2000), Crowley (2000), Shindell et al. (2001a, b), Rind et al. (2004), von Storch et al. (2004) and Stendel et al. (2005). However, it could be argued that these studies are problematic for two reasons. Firstly, a detailed knowledge of the pre-industrial external forcing does not yet exist. This is particularly the case for solar forcing. In recent irradiance reconstructions (Wang et al. 2005) the amplitude of the background component is 0.27 times that of Lean (2000) and consequently smaller than what has been used in previous studies. As a result the total solar irradiance increases by only  $0.5 \text{ Wm}^{-2}$  from the Maunder Minimum to the present-day quiet sun. Secondly, internal processes exercise significant influence on regional climate even on decadal time scales and longer (Wunsch 1999; Vallis et al. 2004; Gerber and Vallis 2005). So even if the climate forcing could be known exactly it will not be feasible to reproduce the regional climate except in a statistical sense.

A minimum condition for reproducing climate variability is that a climate model must be capable of reproducing the characteristic variations in time and space of the general circulation of the atmosphere. This includes a realistic portrayal of ENSO, the NAO and other typical features of the climate system on time scales from days to several centuries. It is also important that such a model has a sufficient resolution to realistically generate tropical and extra-tropical storm

tracks. A climate model, which seems to meet most of these requirements, is the recently developed ECHAM5/ MPI-OM model at the Max Planck Institute for Meteorology, (Jungclaus et al. 2006). This model does not employ any flux adjustment. The model version, which is investigated here, has a high spatial atmospheric resolution for a climate model, as represented by 63 spectral modes with triangular truncation and 31 levels in the vertical (T63L31). It gives a realistic description of the ENSO (van Oldenborgh et al. 2005) and storm tracks (Bengtsson et al. 2006). The model also gives a good description of tropical intra-seasonal variability (Lin et al. 2006)

Here we investigate a 500 year long integration. The experiment has been run with an atmospheric composition typical of the pre-industrial climate. There are no variations in the forcing during the length of the integration so the state of the climate at different times is only a consequence of internal variations of the atmosphere/ocean/land system. In this assessment we will concentrate on the Europe region, as this is an area of the world with several observational records stretching back to the 18th century. These records are also supported by documentary proxy evidence of incidental character (Brazdil et al. 2005 and references therein) even further back in time. We will compare the model result with a recent reconstruction of the surface temperature records over the European land area (35N-70N, 25W-40E) from 1500 onwards for seasonal periods. (Luterbacher et al. 2004; Xoplaki et al. 2005). Those reconstructions are based on long instrumental station series, temperature indices based on documentary proxy evidence, sea ice information from the Baltic Sea and from Iceland as well as high resolution natural proxies such as ice core data from Greenland and tree ring evidence from Scandinavia. For this reason the main emphasis will be on surface temperature, although the model data include a broad range of variables. Further the emphasis is on the climate variability of Europe, but we will explore this in an overall context of global climate variability. We focus here on summer and winter using recent updated data sets provided by Luterbacher (2005, personal communication). In the new data set only temperature predictors have been used for the reconstruction (no pressure), with calibration in the 20th century being done with the new Mitchell and Jones (2005) gridded data, which has somewhat more variability than that of New et al. (2000), which was used in Luterbacher et al. (2004). There are also a few more instrumental predictors mainly from the 18th and 19th century as well as some additional natural proxies for the 1500 to 1650 period. Compared to Luterbacher et al. (2004) this

data set has slightly colder temperatures both in summer and winter.

The main scientific issue of this study is whether the variability of the European climate can be interpreted as essentially being determined by internal processes of the climate system. This will include:

1. What is the typical internal variability of the climate experiment and how is European climate variability related to variability on the global scale?
2. What types of climate trends are due to internal processes?
3. What are the characteristic features of winter and summer temperature in the model including extreme conditions, and how do they compare with observations/reconstructions?
4. What is the typical variability of storm tracks influencing European climate and how are climate anomalies related to the storm tracks?
5. To what extent are sustained climate anomalies in the European region coupled to global or hemispheric modes of circulation such as NAO, PNA or ENSO?

The paper continues with a description of the coupled model in Sect. 2, followed by a discussion of the variability in Sect. 3 and trends in Sect. 4. Storm tracks and NAO are discussed in Sect. 5 and ENSO and PNA in Sect. 6 with extremes in Sect. 7. Finally a discussion of the results is presented in Sect. 8 and final remarks in Sect. 9.

## 2 Description of the model and the experiment

The coupled model used in the experiment consists of new model versions for both the atmosphere and the ocean. In the atmosphere model (ECHAM5; Roeckner et al. 2003, 2006) vorticity, divergence, temperature and the logarithm of surface pressure are represented by a truncated series of spherical harmonics (triangular truncation at T63), whereas the advection of water vapour, cloud liquid water and cloud ice is treated by a flux-form semi-Lagrangian scheme. A hybrid sigma/pressure system is used in the vertical direction (31 layers with the top model level at 10 hPa). The model uses state-of-the-art parameterizations for shortwave and long wave radiation, stratiform clouds, cumulus convection, boundary layer and land surface processes, and gravity wave drag.

The ocean model (MPI-OM; Marsland et al. 2003) uses the primitive equations for a hydrostatic Boussinesq fluid with a free surface. The vertical

discretization is on 40 z-levels, and the bottom topography is resolved by means of partial grid cells. The ocean has a nominal resolution of  $1.5^\circ$  and the poles of the curvilinear grid are shifted to land areas over Greenland and Antarctica. The parameterization of physical processes include along-isopycnal diffusion, horizontal tracer mixing by advection with unresolved eddies, vertical eddy mixing, near-surface wind stirring, convective overturning, and slope convection. Concentration and thickness of sea ice are calculated by means of a dynamic and thermodynamic sea ice model.

In the coupled model (Jungclaus et al. 2006), the ocean passes to the atmosphere the sea surface temperature (SST), sea ice concentration, sea ice thickness, snow depth on ice, and the ocean surface velocities. The atmosphere runs with these boundary values for one coupling time step (one day) and accumulates the forcing fluxes. These fluxes are then transferred to the ocean. In addition to wind stress, heat and fresh water fluxes the 10 m wind speed is passed to the ocean for the calculation of the turbulent wind mixing. All fluxes are calculated separately for ice-covered and open water partitions of the grid cells. River runoff and glacier calving are treated interactively in the atmosphere model and the respective fresh water fluxes are passed to the ocean together with the atmospheric precipitation minus evaporation field. A special feature of the coupled model is that the surface wind stress over the ocean is calculated relative to the ocean current. This considerably reduces the cold bias in the equatorial Pacific. The model does not employ flux adjustments.

The coupled model was run at pre-industrial atmospheric concentrations of carbon dioxide ( $\text{CO}_2$  at 286.2 ppm), methane ( $\text{CH}_4$  at 805.6 ppb), and nitrous oxide ( $\text{N}_2\text{O}$  at 276.7 ppb) for about 500 years. During this time no notable climate drift could be identified in the atmosphere and in the upper part of the ocean. For example, the linear trend in annual global

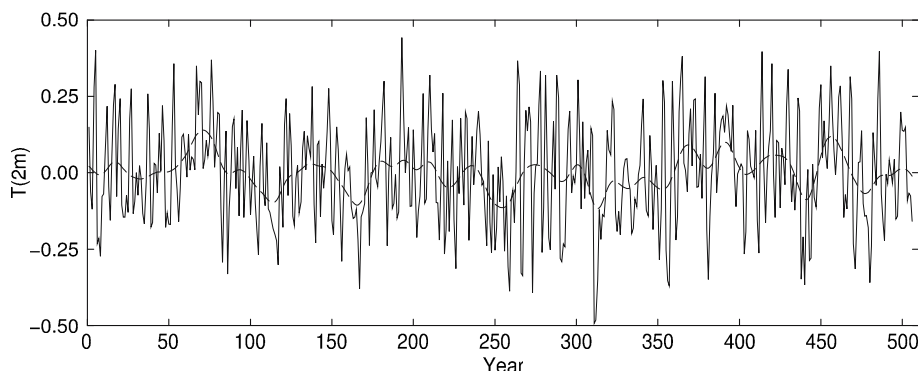
mean surface air temperature was negligibly small ( $+0.027$  K/century).

### 3 Variability of the pre-industrial climate

Based on the model result, the average global surface temperature of the pre-industrial period, computed from the 2 m-temperature field, is estimated to be 0.19 K colder than the climate reference period of 1961–1990 (averaged of three 30 year realizations) and using greenhouse conditions for this period. The European winter temperature is lower by 0.54 K, but the summer temperature is virtually the same as for the late 20th century. As the time of comparison is limited to 90 years only, these differences are only tentative but indicate nevertheless that the simulated pre-industrial climate varied around an average value lower than the present climate and that the colder conditions in Europe were essentially confined to the winter. The global result is consistent with an increase in anthropogenic forcing as used in the model and described elsewhere. However, as our main emphasis is on the variability of the pre-industrial climate and not on absolute values we consider the absolute differences as tentative only. As explained below there is a minor cold bias in the model results compared to the observational estimate.

The de-trended annual global averaged surface temperature is shown in Fig. 1 for the 500-year-period. The difference between the coldest and warmest year is about 0.9 K and the differences of 50 year averages is about 0.25 K. The warm years are generally associated with positive ENSO events. The global mean temperature for the boreal winter, December through February (DJF), has a correlation of 0.70 with the ENSO, NINO3 index computed from the model SST's. This is larger than the observed correlation for the last 40 years as obtained from the ERA40 reanalysis data,

**Fig. 1** Time series of the anomaly of the annual global surface temperature for 500 years for the pre-industrial climate from the ECHAM5/OM1 climate model (*solid line*). The *dashed line* shows the result of applying a 30-year Gaussian smoothing. The data has been de-trended



which amounts to 0.48. The higher correlation in the model could be due to model bias or to the disparity in the length of the periods for the model and ERA40 with ERA40 being much shorter. We will return to this in the discussion. The correlation in the model run between the European land area and the global domain for the 500 years is + 0.31 (0.14 in the short ERA40 data set). For shorter periods of 40 years we obtained values of + 0.10 and + 0.24 for two randomly selected periods. The correlation between the European land area and NINO3 is + 0.03. In the summer, June to August (JJA), the surface temperature correlation between the European land area and the global domain is + 0.12. The winter temperature anomalies in the European region are thus essentially uncorrelated with the global mean temperature in the model experiment and presumably so even in reality.

Figure 2 shows the time series of the surface temperature, averaged over the European land area (as in Luterbacher, 2005, personal communication) for the 500-year model run for each individual winter and summer season respectively and compared with the observational estimates from Luterbacher (*ibid*). The general impression is that the typical variance is rather similar and periods of warm and cold events vary in an apparent non-periodic manner. Mean values, standard deviations, maximum (warmest season in the whole data set) and minimum (coldest season in the whole data set) values are shown in Table 1 compared with Luterbacher (*ibid*) for 1500–1900. This shorter period of Luterbacher's data is used to exclude the impact of global warming in this comparison. The difference, model-observations/reconstructions, is negligible in both winter and summer. The standard deviation is slightly larger in the model run, presumably due to insufficient variance in the earlier “observed” data. For the last 100 years the observed data has a variance similar to the model results. We have also calculated the extreme seasonal values and note that the range (warmest–coldest) is higher in the model data. This is most pronounced in winter and largely due to a small number of very cold and very warm winters in the model results compared to the reconstructions. Both in the model and the data the extreme seasons and the extreme year do not occur in the same period but are well separated and occur in fact often in different centuries. This underpins the impression that the variations, including the extreme cold and warm seasons, are dominated by internal chaotic processes and unlikely to be reproducible. Next we will explore whether the anomalies of the model integrations indicate typical longer-term structures showing up as regional trends for different periods of time as well as

exploring the relation between surface temperature and other climate variables.

#### 4 Typical climate trends

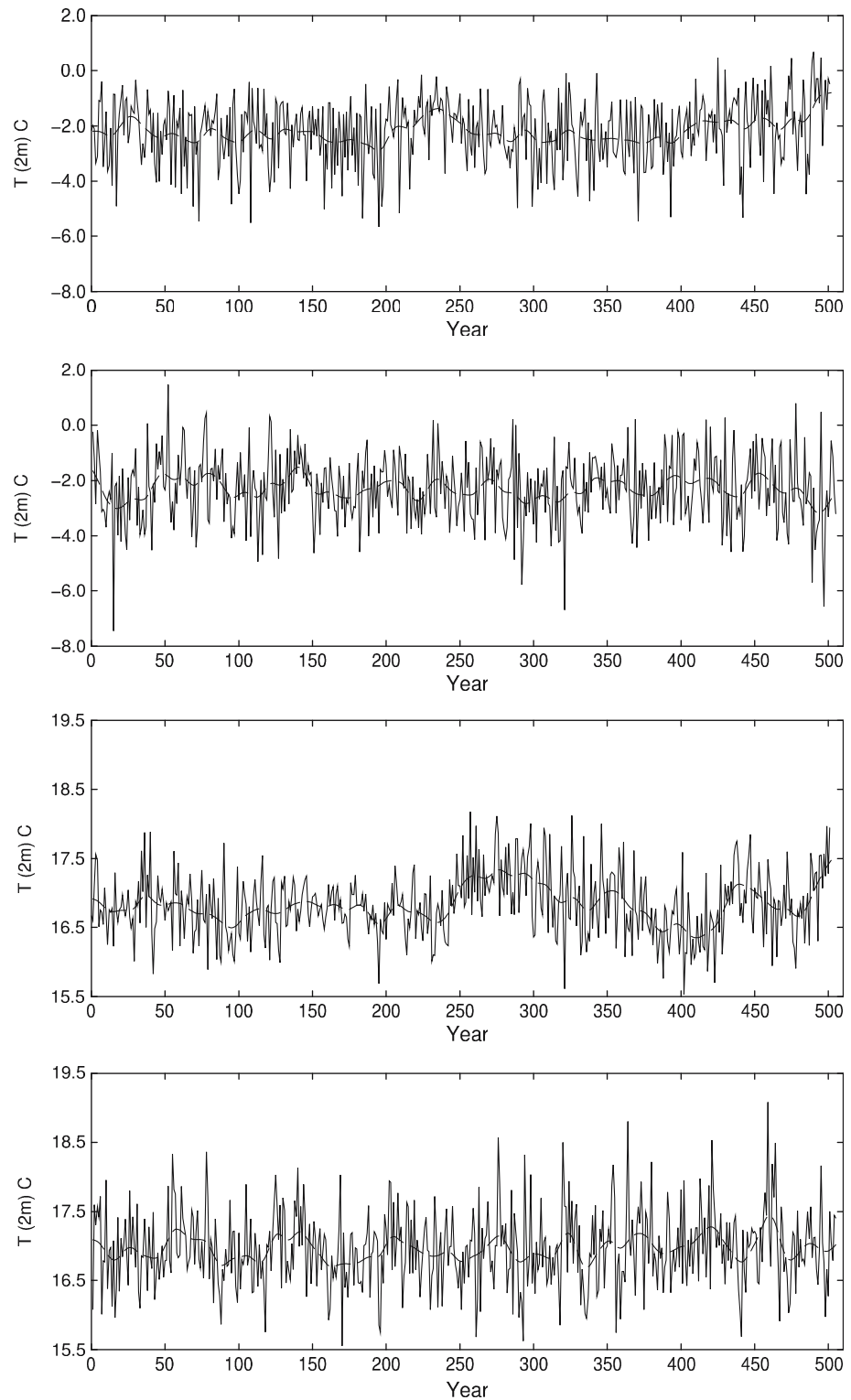
As a suitable starting point for examining trends in the model data, we examine characteristic climate trends of the integration in the identical way to Hunt and Elliot (2006). Trends with durations of 10, 30, 50, 100 and 300 years have been calculated centred on the years 150 and 300, respectively. As in Hunt and Elliot (2006) there is a mixture of co-existing positive and negative trends across the Earth, suggesting multiple internal mechanisms, simultaneously at work in the climate system. Regional, significant trends, as defined and used by Hunt and Elliot (2006), occur for all parameters and for periods at least up to 100 years. At 300 years there are hardly any significant trends to be found. As in Hunt and Elliot the trends have a coherent structure and cover areas of up to some  $20 \times 10^6 \text{ km}^2$ , suggesting marked circulation regime trends.

Trends for surface temperature, precipitation, 850 hPa height field and sea ice are shown in Fig. 3 for the Northern Hemisphere (NH) during the winter December–February (DJF). These are 50-year trends centred on the year 150 showing a cooling trend for Europe. The temperature trend has a marked north-south temperature gradient stretching from Western Europe towards central Siberia with a cooling trend in the north and a warming trend in the south. The precipitation trend is consistent with the temperature trend and shows increasing values in a band through central Europe eastward. Such a trend pattern is associated with a change in the storm track towards a more southerly position over the European region. It is also associated with a weakening trend in the NAO as indicated in the 850 hPa height field (reduced north-south gradient over the eastern north Atlantic) shown in Fig. 3d. The Arctic sea ice, Fig. 3c, shows an increase in most regions, but a decrease in the Labrador Sea. Absolute changes above 0.23 are significant at the 95% level as in Hunt and Elliot (2006). Regional trends longer than 100 years are generally rather weak and insignificant.

#### 5 Variability of the NAO and extra-tropical storm tracks

The NAO has been computed for the model using the difference in area weighted region averages of the

**Fig. 2** Time series of the mean surface temperature for summer and winter for the European land area (35N–70N, 25W–40E) compared to Luterbacher (whole time series). Temperatures are in °C. **a** Luterbacher, DJF, **b** model, DJF, **c** Luterbacher, JJA, **d** model, JJA. The *dashed line* shows the result of applying a 30-year Gaussian smoothing. There are different vertical scales for winter and summer, respectively. Year 0 in Luterbacher refers to AD 1500



DJF averages of geopotential at 500 hPa for regions (35–45N, 10–70W) and (45–70N, 10–70W), (first region–second region). The chosen regions are based on those of Barnstone and Livezey (1987) and can be considered to be a better measure of NAO than the more

traditional difference in pressure between single point values. The NAO time series is centred and normalized and is shown in Fig. 4. This highlights that the NAO undergoes typical irregular variations ranging from a maximum index value of 3.2 and a minimum

**Table 1** Mean value, standard deviation, and extreme temperature for model and observed data

	Luterbacher (2005) <sup>a</sup>			Model <sup>b</sup>		
	Annual	DJF	JJA	Annual	DJF	JJA
Mean	8.13	−2.31	16.83	7.39	−2.30	16.96
SD	0.41*	1.15	0.47	0.55	1.23	0.55
Min. Year	6.61 (1695)	−5.69 (1695/96)	15.62 (1821)	5.41(16)	−7.45 (15)	15.55 (170)
Max. Year	9.40 (1822)	−0.09 (1842/43)	18.18 (1757)	9.41(78)	1.47 (52)	19.08 (459)
Max.–Min.	2.79	5.60	2.56	4.00	8.92	3.53

\*Standard deviation for the last 100 years is 0.53 suggesting that the variance is underestimated in the earlier data records. Units in K

<sup>a</sup>Observed land surface temperature 1500–1900 for the European land area (35N–70N, 25W–40E according to Luterbacher (2005))

<sup>b</sup>The same for the ECHAM5/ MPI-OM integrated and initialized under pre-industrial forcing

value of  $-2.45$  standard deviations. As can be seen from the smoothed curve there are also some periods of about 50 years, which are dominated by positive values, and there are longer periods when negative values dominate. There are also indications of longer periods with smaller inter-annual variability and others with larger. In Fig. 5 composites of the cyclone track density for DJF are shown for all cases above and below two standard deviations of NAO. These are computed using the same cyclone tracking analysis used by Hoskins and Hodges (2002) and Bengtsson et al. (2006) applied to the lower tropospheric relative vorticity at 850 hPa ( $\zeta_{850}$ ). As shown in Bengtsson et al. (2006, their Figs. 2 and 3) the modelled storm tracks agree well with ERA40 reanalyses. The positive phase of NAO (Fig. 5a) coincides with an active northerly storm track over the North Atlantic and the northern United States and Canada and a weaker storm track over the Mediterranean. The centre of cyclogenesis over Alberta (Fig. 5c) is also more enhanced. The storms also reach their maximum intensity in a more easterly position (Fig. 5a) thus contributing to the intensity of the Icelandic Low (Loptien and Ruprecht 2005). During the negative NAO phase (Fig. 5b) the Atlantic storms are in a more southerly position around 45N. The mean intensities of storms reflect this change in orientation (Fig. 5b). Between Scandinavia and Greenland the storm track activity is significantly reduced but significantly enhanced over the Mediterranean region. Such a configuration favours outbreaks of cold continental air in winter as well as conditions with high-pressure centres over Northern Scandinavia typical of cold European winters. Areas of cyclogenesis differ somewhat (Fig. 5d) and the region of major cyclogenesis over North America is generally more active in the more southerly centre over Colorado and New Mexico. The cyclogenesis centre on the United States east coast is also in a more southerly position

and weaker. There is also more secondary cyclogenesis coincident with the more southerly storm track.

There is a high correlation between the position of the Atlantic storm tracks and the European climate. A southerly storm track in winter makes it possible for cold continental air to invade the northern and central part. A cold winter is further enhanced through feedback from snow-covered land and extended sea ice cover in the Baltic Sea, (e.g. Koslowski and Glaser 1999). The correlation between NAO and the European winter surface temperature of the model is 0.46. The correlation is higher with the northern region, being reduced to a negative correlation in the most southern part.

## 6 ENSO and PNA

As discussed in van Oldenborgh et al. (2005), the coupled ECHAM5/MPI-OM has a realistic description of ENSO although with a slightly higher anomaly than in observations. The characteristic of ENSO in the pre-industrial run is similar to the present climate. As shown in Fig. 6 for the average NINO3 index (centred and normalized) during DJF, it is interesting to note that extreme ENSO events can be absent for centuries and then be common for some periods such as between years 260–360 when four marked warm events that reached well above  $+3$  K (in the un-normalized index) occurred. This suggests that ENSO in the model has a considerable low frequency variability of an aperiodic nature, as noted in specific studies of ENSO (Zebiak and Cane 1987). As mentioned above there is a strong correlation between ENSO and the global average surface temperature amounting to 0.70. This is larger than in the latest observational data in ERA40.

For Europe however, there is only a modest climate influence of ENSO except a minor negative correlation

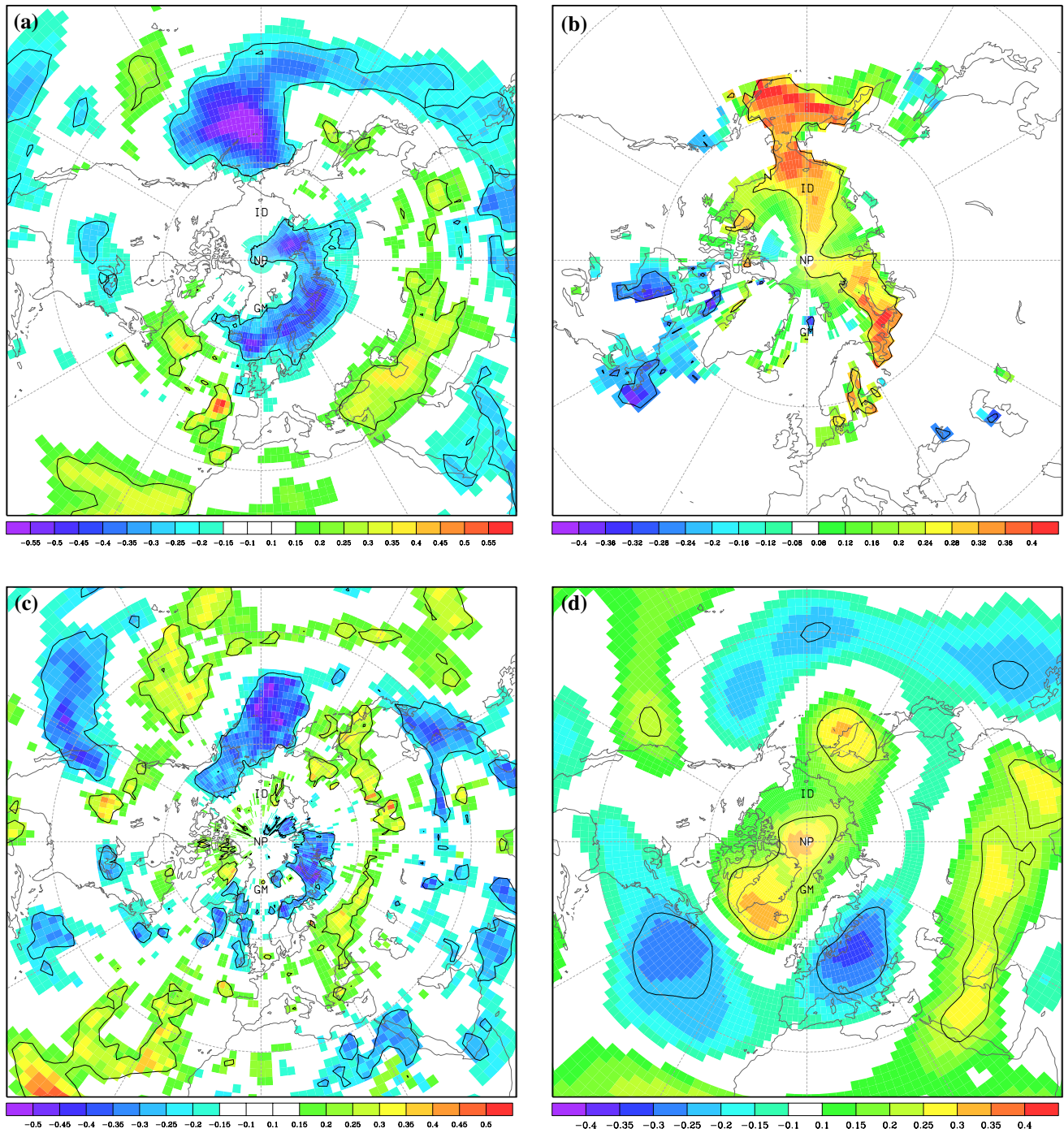


**Fig. 3** Trends for DJF of selected variables calculated for the years 125–175 of the pre-industrial integration presented as correlation coefficients. **a** 2 m temperature, **b** Arctic sea ice, **c**

precipitation and **d** height field at 850 hPa. The full line indicates 95% significance

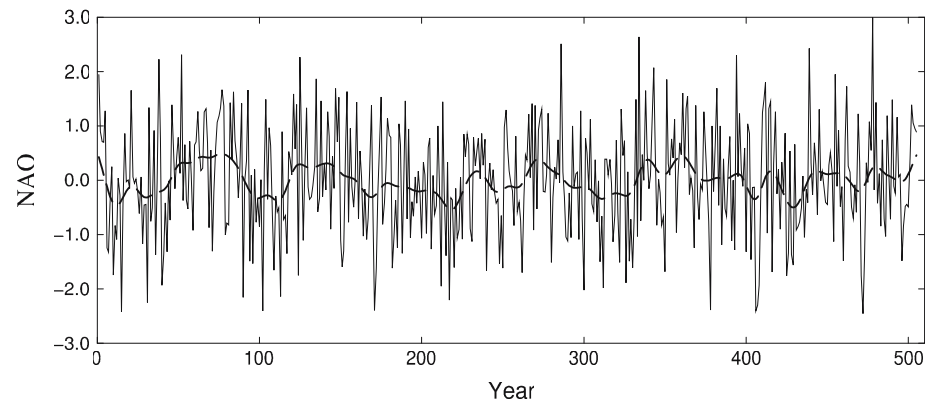
with the DJF temperature anomaly. This is supported from observational studies (Fraedrich and Müller 1992), which indicate a preference for a negative correlation. For the 20 coldest winters in Europe the correlation is  $-0.29$ . We do not consider this as

significant as the correlation is both less for the 10 coldest and for the 30 coldest winters.

We have also calculated the PNA pattern (not shown). This pattern is well correlated with ENSO showing a large variability in the model years 260–360.



**Fig. 4** Model calculation of the NAO for the DJF period, centred and normalized. The *dashed line* shows the result of applying a 30-year Gaussian smoothing



There is little if any correlation with the European surface temperature.

## 7 Extreme winter and summer climate

In this section the coldest European winter and warmest summer for the model are compared globally with the Goddard Institute for Space Studies (GISS) global temperature analyses (Hansen et al. 2001). The data set from Luterbacher (2005, personal communication) is used to choose the observed coldest European winter and warmest summer. The coldest European winter in Luterbacher's data set is the winter 1695/1696. However, an almost equally cold winter in Luterbacher's data for Europe, which overlaps, with the GISS data is that of 1941/1942. The global surface temperature anomaly for this year is shown in Fig. 7a from the GISS data. We compare this with the coldest European winter in the 500-year model run as a global map and shown in Fig. 7b. The coldest model winter is in many respects similar to the winter 1941/1942. The cold anomaly covers the whole of Europe except Iceland with the largest amount in southern Finland eastern Russia and the Baltic states, where it reaches some 7 K. There was a marked El Niño in the winter of 1941/1942 and this was also the case in the cold model winter. The global temperature anomaly pattern in the model run has many similarities to the 1941/1942 winter with positive temperature anomalies over Alaska and western Canada, typical of a warm ENSO event (Brönnimann et al. 2004; Brönnimann 2005).

Next we compare the warmest model European summer shown as a global map in Fig. 7d, with the summer of 1947, identified in Luterbacher's data as the second warmest European summer in the 20th century and one of the warmest in the 500-year data set. This is shown as a global temperature anomaly map using the GISS data in Fig. 7c. There are many similarities between the model and observed temperature maps, in

particular over Eurasia. There are negative temperature anomalies over Alaska and western Canada and both model and observations indicate a cold ENSO event. Although these results cannot be fully convincing, it nevertheless demonstrates that the model can simulate extreme regional anomalies.

In order to obtain a more robust result of extreme European winter and summer the ten coldest European winters and the ten warmest summers are selected in order to compare with similar results presented by Luterbacher et al. (2004). Composites for the ten coldest European winters from the model and Luterbacher are shown in Fig. 8a and b respectively. These show that there are considerable similarities between the model results and the Luterbacher data set both in amplitude and distribution. The model anomaly patterns are in a slightly more southerly position, but cover similar geographical areas. As the extreme seasons are taken from the whole data set it is not possible to compare with global observations.

The global temperature anomalies from the model run as well as the NH 500 hPa height fields have also been computed for the same 10 coldest model European winters. These are shown in Fig. 8c and d respectively. The global surface temperature pattern is rather similar for most of the extremely cold European winters, with a cold anomaly pattern stretching eastward into central Russia. The most eastern part of Russia and Alaska is warmer than normal, but with an indication of a modestly cold anomaly over the central United States. In spite of the fact that there is only a weak negative correlation between European winter anomalies and NINO3 it appears that several of the extremely cold European winters have a warm central tropical Pacific as can be seen in the mean of the coldest ten winters. The NH 500 hPa pattern shown in Fig. 8d has a more southerly position of the jet over the eastern Atlantic and Europe with a marked ridge over the Norwegian Sea. A more detailed analysis indicates more blocking highs than normal west of Scandinavia.

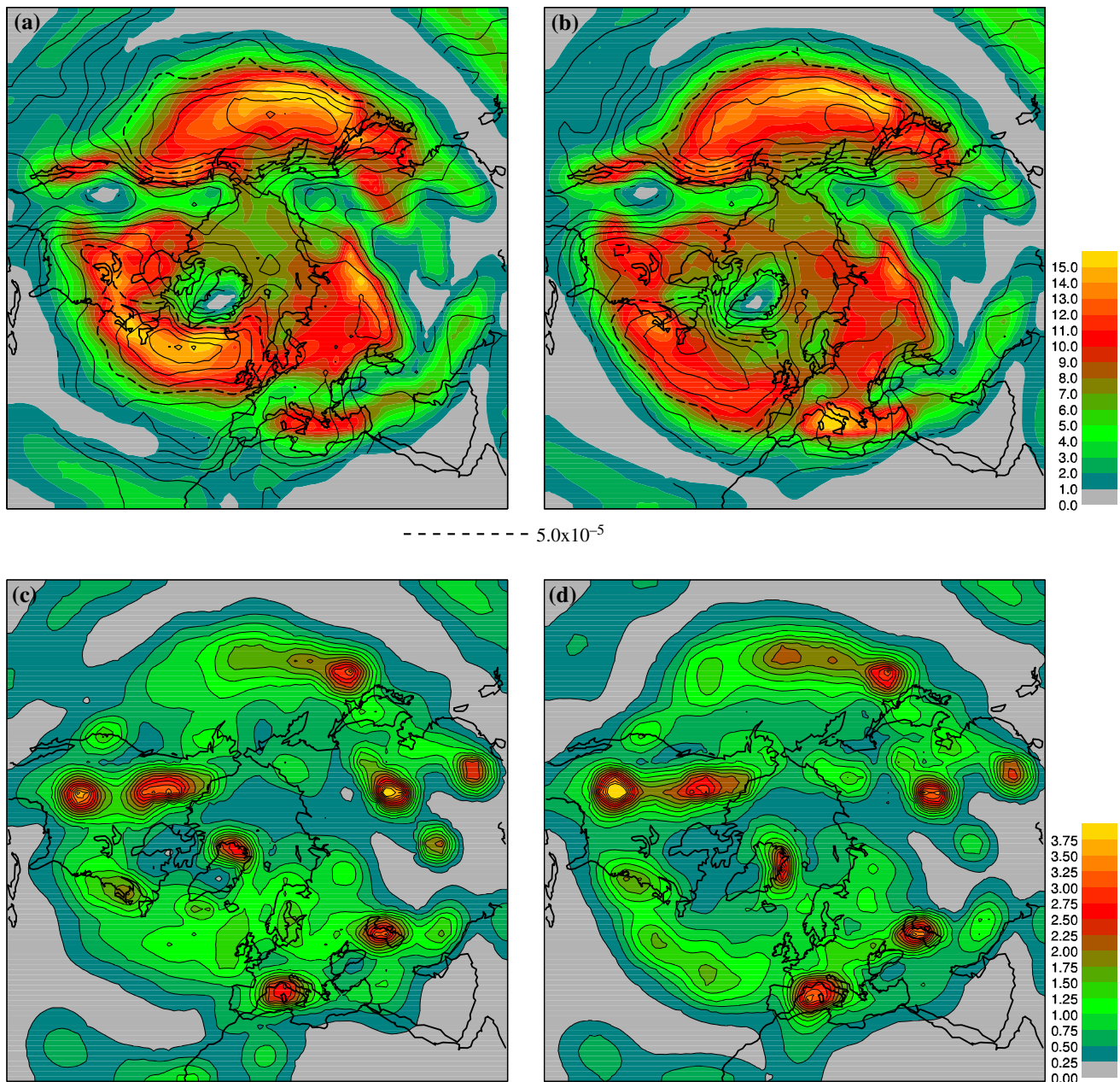


**Fig. 5** Northern Hemisphere cyclonic storm track composite statistics based on  $\xi_{850}$  for DJF periods where NAO  $\geq 2$  standard deviation and NAO  $\leq -2$  standard deviation. **a** Track density (colour) and mean intensity (line) for NAO  $\geq 2$ , **b** same as (a) but for NAO  $\leq -2$ , **c** cyclogenesis density for NAO  $\geq 2$ ,

**d** cyclogenesis density for NAO  $\leq -2$ . Densities are number density per month per unit area where the unit is equivalent to a  $5^\circ$  spherical cap ( $\sim 10^6 \text{ km}^2$ ) and mean intensity is in units of  $10^{-5} \text{ s}^{-1}$  with a contour interval of  $0.25 \times 10^{-5} \text{ s}^{-1}$

Also calculated but not shown is the difference in the 500 hPa pattern for the ten coldest –ten warmest winters, which indicated an overall weakening of the westerlies around 50–60 N and an enhancement of the westerlies around 30 N.

For the ten warmest European summers, Fig. 9 shows the average of the ten warmest summers in the model experiment and the observations of Luterbacher.

The patterns are rather similar, but with the model showing a more south-easterly position of the peak temperature. Mean values and extreme values are similar. The global temperature anomaly pattern for the ten warmest European summers is shown in Fig. 9c. The warm anomaly is mostly confined to Europe but a pattern of higher than normal values can be found over northern Russia. Alaska with northern Canada being

**Fig. 6** Centred and normalized NINO3 index as a measure of ENSO computed from the model SST's averaged over DJF periods. The dashed line shows the result of applying a 30-year Gaussian smoothing

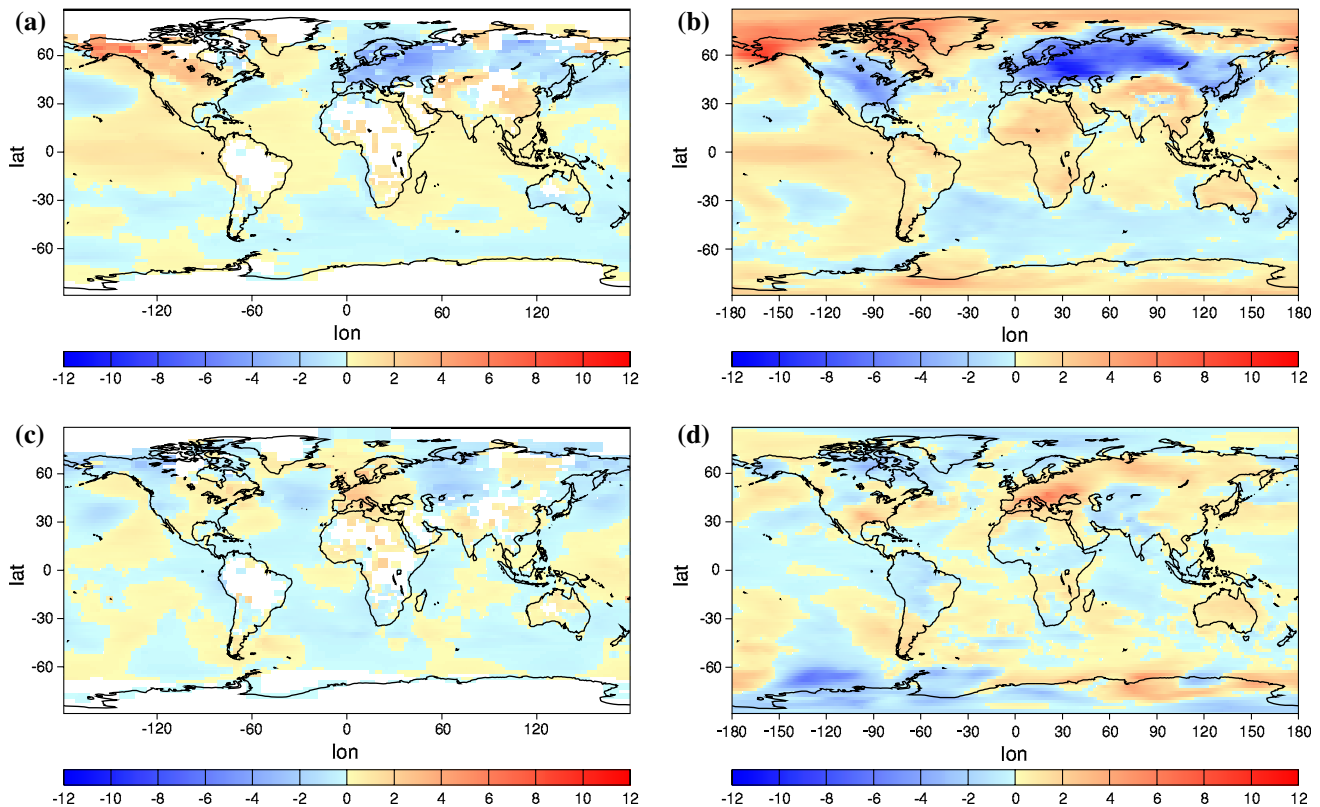
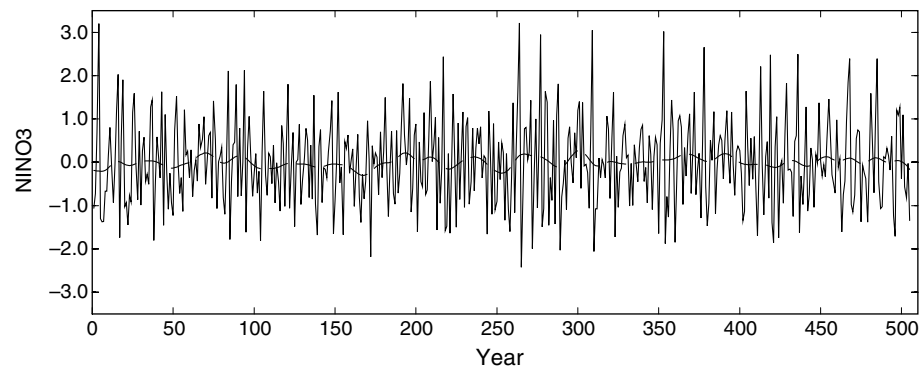


**Fig. 7** Global 2 m temperature anomaly maps for **a** the observed winter 1941/1942 (DJF) using 1951–1980 as the base period from the GISS data, **b** the coldest model European winter (DJF), deviations from the 500 year winter average, **c** observed summer

1947 (JJA) using 1951–1980 as the base period from the GISS data, **d** the warmest model European summer (JJA), deviations from the 500 year summer average

colder than normal. Also, colder than normal values can be found over the central and western tropical Pacific. For the extremes most of these patterns can be identified in the majority of the extreme warm summers. The 500-hPa height field has only minor anomalies (Fig. 9d) but there is a marked divergent flow over Europe suggesting subsidence over the region.

Finally, in order to explore the structure of persistent temperature anomalies we calculate the European coldest and warmest *consecutive* 30-year

periods respectively for winter and summer. Results for these are shown in Fig. 10a–c and Table 2 for the difference between the coldest and warmest winter periods from the model and from the Luterbacher data set. We have here excluded the observed data for the 20th century as the steadily increasing anthropogenic forcing influences the longer-term trends. Again the temperature differences are similar both in amplitude and distribution, but with a slight northward position of the model pattern. We believe

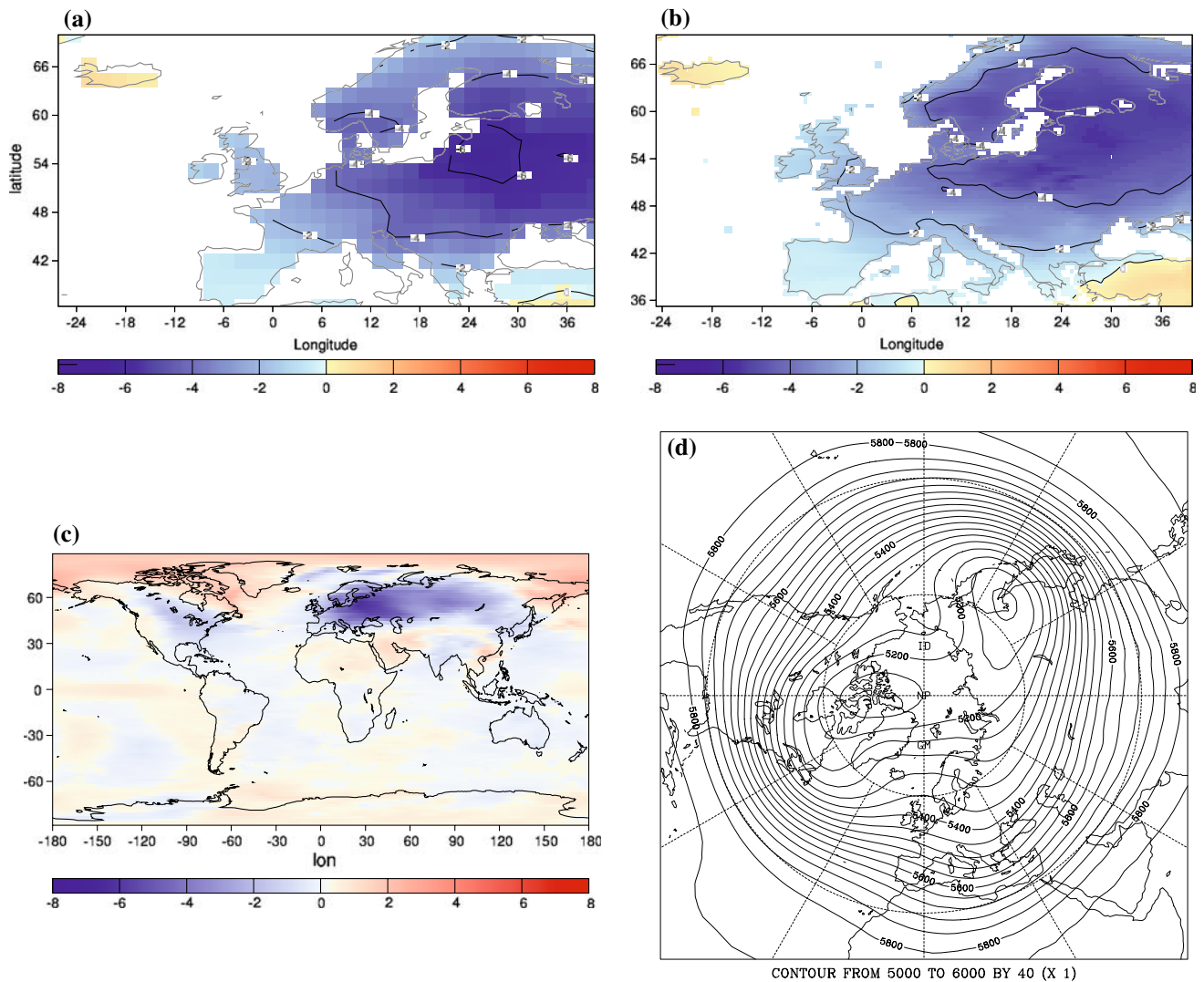


**Fig. 8** Coldest ten European winters **a** model 2 m temperature anomaly ( $^{\circ}\text{C}$ ), **b** observations, temperature anomaly from Luterbacher, 1500–1900, ( $^{\circ}\text{C}$ ), **c** model, global surface tempera-

ture anomaly for the same years ( $^{\circ}\text{C}$ ), and **d** model NH 500 hPa geopotential field (gpm) for the same years. Isolines for  $-2$ ,  $-4$  and  $-6^{\circ}\text{C}$  are indicated in (a) and (b)

this suggests that multi-decadal climate anomalies are likely to be due to internal processes and do not really require changes in the external forcing. The corresponding global surface temperature patterns (not shown) indicate substantial areas where the difference is larger than 1 K with the north-eastern Europe larger than 2 K. The largest value 5.6 K occurs in the Barents Sea region and is related to variations in the sea-ice cover. We have also inspected the storm track differences between the two 30-year periods. Differences are relatively small but in the colder period the Atlantic storm track is in a more westerly and southerly position (not shown).

Similarly Fig. 10d–f and Table 2 show the difference between the warmest and coldest 30 consecutive

European summers. Here the observed anomalies in Europe are larger than found in the model, as the model does not reproduce the high observed values over Scandinavia. It is not clear whether this is due to external forcing differences (volcanic aerosols for example) or whether it reflects a deficiency of the model to reproduce the low-frequency variance of the summer climate. We believe the latter is the most likely cause as the extreme pattern is so geographically limited that it is unlikely that external forcing only had influenced this small region. One possible cause could be influences of the surface water temperature in the Baltic, which is insufficiently handled in the model. Similarly the height of the Scandinavian mountains is significantly reduced in the model due to insufficient

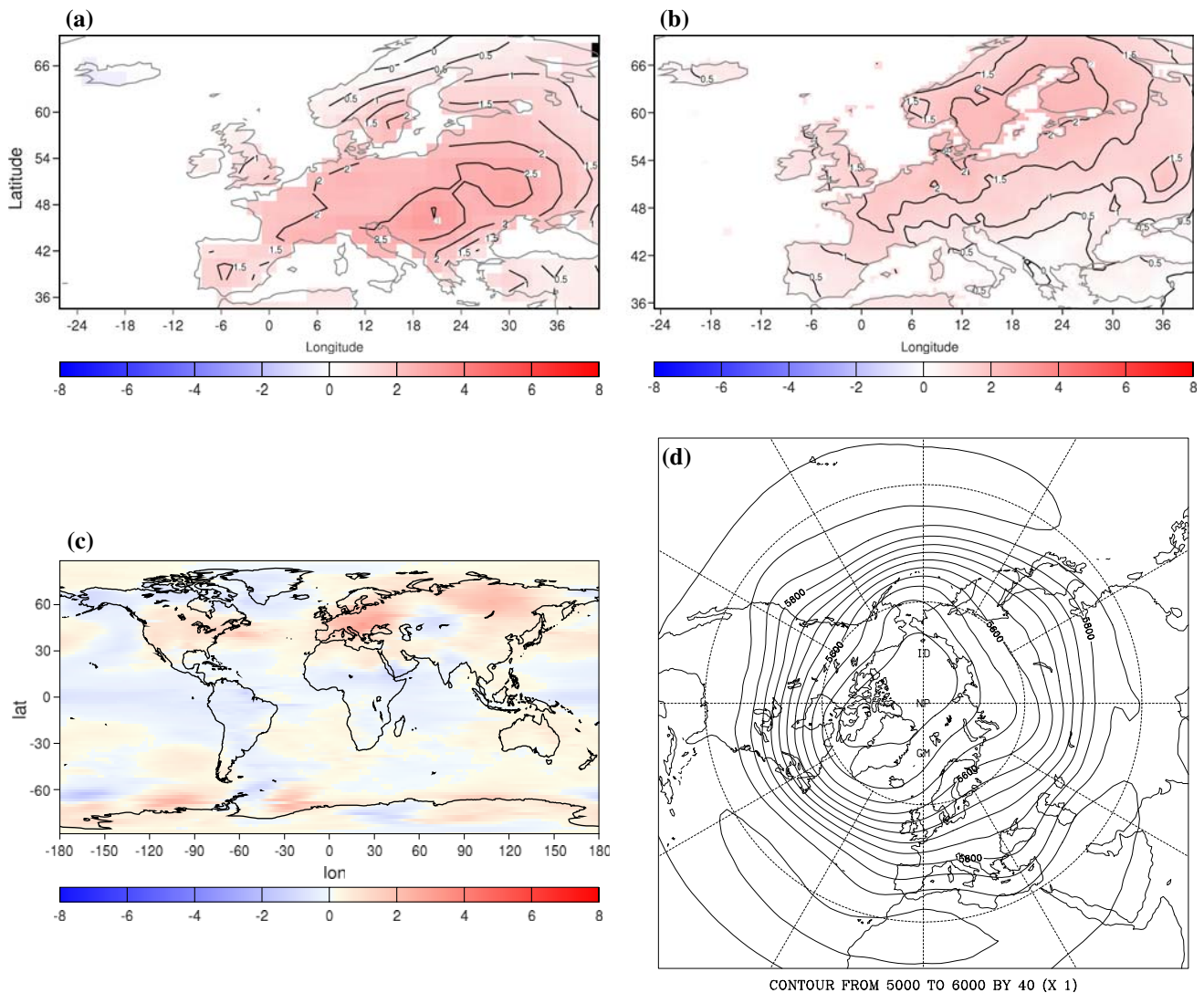


**Fig. 9** The same as Fig. 8 but for the warmest ten summers. Isolines for every 0.5°C between 0 and +3°C

resolution, which could effect the blocking high over Scandinavia.

## 8 Discussion

We have organized this investigation along a similar line to the recent empirical study by Luterbacher et al. (2004) in order to compare with an available observational reconstruction of the European climate for the period 1500–1900. This data set includes one of the longest and presumably most reliable observational records from any parts of the world. We have restricted the presentation to averaged values for the European land area although we have also examined several available local records. We have also limited the intercomparison to winter and summer. The modelled surface temperature

has a minor cold bias and has slightly higher variance than the observed data. The smaller variance in the observational data is due to reduced variance in the earlier years when data coverage is likely to be poorer. The temperature range especially in winter is higher in the modelled results. However, this is mainly due to a smaller number of extreme winters not found in the observational reconstructions.

There are considerable regional anomalies over several decades in the model run creating by chance extremely cold and warm seasons as well as longer periods when the average values differ from another equally long period with an amount very similar to the latest available long-term observational reconstruction of the seasonal climate of Europe. This suggests that external influences (volcanic aerosol, solar forcing, etc) have had very little influence on the European climate.

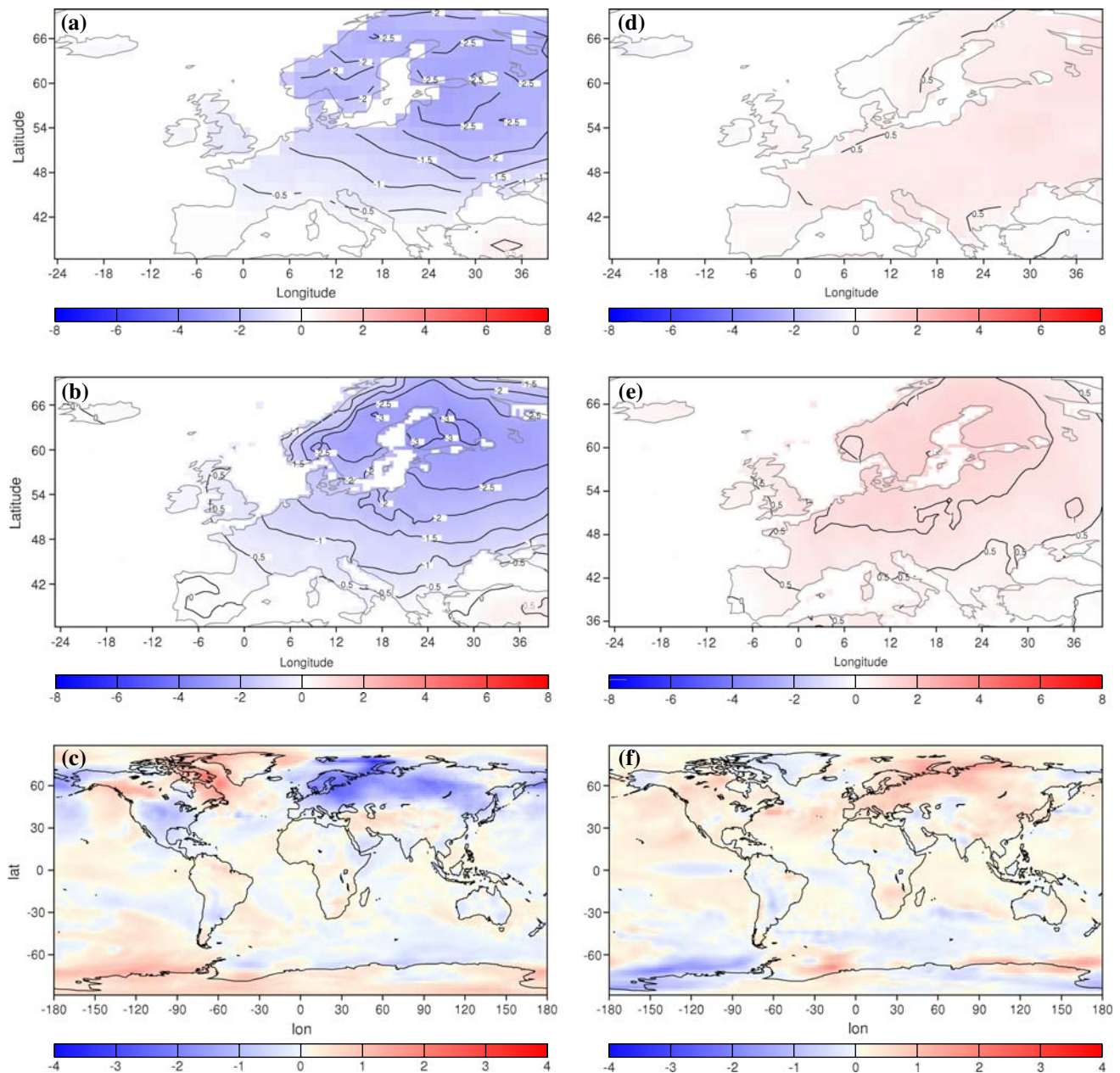


**Fig. 10** **a** Surface temperature differences for 30 consecutive European winters from the model, coldest-warmest, **b** surface temperature differences for 30 consecutive European winters from observations of Luterbacher, 1500–1900, coldest-warmest, **c** global surface temperature differences for 30 consecutive European winters from the model same periods as in (a), coldest-warmest. **d** Surface temperature differences for 30

consecutive European summers from the model, warmest-coldest, **e** surface temperature differences for 30 consecutive European summers from observations of Luterbacher, 1500–1900, warmest-coldest, **f** global surface temperature differences for 30 consecutive European summers from the model same periods as in (d), warmest-coldest. Isolines for every 0.5°C are indicated in the regional maps

This is further supported from Table 3 where we have summarized the extreme seasons and extreme decades for the results of Luterbacher et al. (2004) and Xoplaki et al. (2005). It appears reasonable to assume that in the case of a major external forcing that the extreme seasons would occur in the same year (it is interesting to note that the only exception here is the warming at the end of the 20th century). However, extreme

seasons actually occur in very different periods suggesting a domination of internal processes rather than external forcing. There have been several attempts made in the past to reproduce the past European climate using an anticipated forcing from all possible sources, for example, Zorita et al. 2004, Stendel et al. (2005). We do not consider this very likely to succeed for two different reasons. Firstly, because the forcing

**Table 2** Surface temperature difference between the coldest and warmest 30-year consecutive winters (DJF) and the difference between the warmest and coldest 30-year consecutive summers (JJA)

Season	Luterbacher (2005)		Model	
	DJF	JJA	DJF	JJA
Mean	−1.23	0.71	−1.27	0.52
Extreme	−3.09	1.53	−2.84	0.99

Mean is the average for the European land area and Extreme is the grid point value with the greatest difference. Units in K

from volcanic aerosols and solar forcing are not very accurate, in particular for the solar forcing. Secondly, the response to forcing is essentially determined by the pattern of response rather than the pattern of forcing (Boer and Yu 2003a, b) making it very difficult to attribute a specific response pattern to a specific forcing pattern in a small region such as Europe. Consequently we do not consider it feasible to compare the time evolution of simulated records with observed records. A more realistic comparison can be made only with the statistics of climate.

What could then have been the cause of extreme climate episodes in the pre-industrial European climate? Firstly, the climate has varied around a climate colder than the present due to less greenhouse gases. The model result suggests that the pre-industrial climate has varied around a winter temperature some half a degree colder than the climate for 1961–1990. This would have made it possible to experience extreme winters at least lower than the coldest seasons in the period 1961–1990. During 1961–1990 there were a number of extreme seasons in Europe including excessively cold winters. The intercomparison also includes periods of 30 years duration having an average winter temperature of 1.27 K colder than the warmest 30-year period in close agreement with observed estimates, see Table 2.

There is an almost equally good agreement of the extreme summer temperatures except the longer period of 30 years have less variance than the model result.

**Table 3** Compiled data from Luterbacher et al. (2004) and Xoplaki et al. (2005) covering the period 1500–2003

	Coldest year	Coldest decade	Warmest year	Warmest decade
Winter	1695/1696	End 1600	1990	1990s
Spring	1785	Around 1700	1989	1990s
Summer	1902	Beginning 1900	2003	1990s
Autumn	1912	End 1800, early 1900	1938	1930s

The table shows the years and decades of the coldest and warmest seasons, respectively

In the observational reconstruction this is due to the large difference between the relative warm period during the second half of the 18th century and the colder period from the end of the 19th century stretching into the first part of the 20th century. In comparison the reconstructed summer temperatures prior to 1750 or so has only minor fluctuations. We are presently not able to explain this and believe the further studies be carried out both in the observational reconstruction and additional model experiments.

## 9 Concluding remarks

There are significant regional trends in the model integration on the time scale of up to 50 years. These trend patterns are internally consistent suggesting there are organized regional circulation patterns. The temperature difference between the warmest and coldest winter in the model experiment for the European land area is 8.9 K. The corresponding summer value is 3.5 K. The model range is higher than the observational reconstructions, which either could be explained by a model bias or observational bias to capture extreme temperatures. Comparison with selected individual stations having observational records of the order of 200 years (not shown) suggest a larger similarity with model results indicating that the reconstructions have underestimated the extreme values.

The extreme seasons in summer and winter have distinct anomaly patterns. During a cold European winter the storm tracks and jet stream are in a southerly position providing frequent invasion of Arctic air masses over Northern Europe. An extremely cold winter is often associated with a warm ENSO event and is similarly suggested from observations of cold winters over the last century. There are also indications that this has also occurred in other previous centuries. The amplitude and relative frequency of extreme seasons in the model runs are similar in amplitude and extension to the observations. This suggests strongly that internal dynamics of the coupled climate system is the dominant cause of regional climate variations.

There are sizeable differences between the coldest and warmest consecutive 30-year periods, respectively which means that such periods of time can be dominated by colder or warmer climate due to internal climate processes. The model differences are very similar to the observed differences but the observed anomalies are larger in the summer. The main cause to the deviation from the model run is the large difference in summer temperatures in the second part of the 18th

century and the comparative cold period in the late 19th century and early 20th century in the observational reconstruction. Such large changes in the summer temperatures cannot be seen in the observational reconstructions prior to the middle of the 18th century. We have no explanation to this but it could be an indication of inconsistencies in the data used in the reconstructions.

The lack of low frequency variability in summer temperatures in the model could be due to forcing factors not included in the model. This may include stratospheric aerosols from volcanic eruptions and/or land surface changes. Other alternatives are insufficient treatment of land surface processes in the model such as deficiencies in the treatment of evapotranspiration, which are likely to influence summer temperature.

It seems from an assessment and intercomparison of observed and modelled data sets that there is little support to hypothesize a possible external forcing such as from low frequency solar variability. Volcanic eruptions have been documented but it seems that the overall effect on climate variability for this period is limited. This is supported from the latest regional climate assessment for Europe (Luterbacher et al. 2004; Xoplaki et al. 2005) where extreme climate conditions for different seasons do not coincide (Table 3). These studies support the claim that the so-called Little Ice Age was not a coherent period but rather several shorter periods of colder weather than normal. We also note that the cold episode associated with the Maunder Minimum in the late 17th century was not confined to all seasons as the temperature both in summer and autumn were colder at the end of the 19th century and early 20th century (Luterbacher et al. 2004; Xoplaki et al. 2005).

There are possible physical mechanisms of the coupled climate system, which are capable of generating low frequency variability affecting the European climate. As first suggested by Hasselmann (1976) a white spectrum generated by transient synoptic eddies is a priori reddened due to stochastic processes. This is a possible mechanism for influencing the NAO as has been convincingly demonstrated by Wunsch (1999). A similar interpretation of Hasselmann's result, but including ocean feedback, has been suggested by Manabe and Stouffer (1996).

Results presented here are naturally model dependent and it cannot be ruled out that other models may arrive at different conclusions. This is likely to be the case if such models have a reduced internal variability on annual to multi-decadal time-scales. If so it is the unresolved variability that is likely to be ascribed to external forcing. However, it now appears that several

of the models used for the 4th IPCC assessment (Overland, 2005, personal communication) have a similar high regional internal variability in extratropical areas as the model investigated here. Another caveat is the reliability of the data set. As was highlighted in Luterbacher et al. (2004) there are considerable error bars in the reconstruction of the seasonal temperatures in particular before 1700.

We have here confined the study to the European land area in view of the fact that this is probably the region with the most accurate long-term meteorological records. However, this is also a region where internal variability is high and it is not unlikely that result may be different in other geographical regions with higher signal to noise ratio. Crowley (2000) who used an energy balanced model concluded that 41–64% of the total variance of the Northern Hemisphere surface temperature could be attributed to forcing. Experiments with the HadCM3 model (Collins et al. 2002) broadly support this. For this reason we strongly suggest that a more extensive study along the line of this study be extended to a few selected models and some additional data reconstructions. Such a study should further be extended to other areas of the Earth where reliable long data records or reliable data reconstructions are available.

Although ECHAM5/MPI-OM is among the models with the most realistic representation of ENSO (van Oldenborgh et al. 2005), the amplitude of the oscillations is higher than observed (Jungclaus et al. 2006). However, this could imply a modest bias towards larger inter-annual variability of the global temperature but presumably not for the European region in view of the weak correlation to the global temperature.

We have not included any variation in the aerosol concentration neither from natural or anthropogenic origin. Several major volcanic eruptions are known in the period 1500–1900, but our experience from Pinatubo and El Chichon is that the influence from such eruptions are limited in time and may at most have influenced the climate for a few years. If anything we would argue that volcanic aerosols would have implied enhanced climate variability particularly during the summer. Anthropogenic aerosols are likely to mainly have had a local influence and may have influenced individual observational records. However, there are no observational reports of any systematic variability in aerosol emission in the period 1500–1900.

As indicated in the introduction we have deliberately excluded any solar influence, as there are no independent records, which prove that such variations in solar irradiation have taken place. Present available data sets of low frequency variability is not inferred



from observational records but are rather hypotheses from analogues with other stars or based on correlation between solar irradiation and sun spots. Recent studies regrettably do not any longer support such claims although low frequency solar forcing cannot be excluded a priori. However, a justification of solar variability as a kind of residual forcing appear hardly to be required as we are able to demonstrate that modelled internal variability is sufficient to match the observed variability for the European region in the most important aspects. For the moment at least we believe it is sensible to apply the principle of *Occam's razor* and consider internal climate variability as a dominant mechanism.

**Acknowledgments** The authors would like to thank Dr. Jürg Luterbacher and Dr. Elena Xoplaki for providing the observed gridded European temperature data used in this study and the Goddard Institute for Space Studies for making the GISSTEMP data available online. We also thank Dr. Luterbacher for providing helpful comments to the manuscript. This research was financed in part by the German Ministry for Education and Research (BMBF) under the DEKLIM project. The simulations were performed on the NEC SX-6 supercomputer installed at the German Climate Computing Centre (DKRZ) in Hamburg.

## References

- Barnston AG, Livezey RE (1987) Classification, seasonality and persistence of low-frequency atmospheric circulation patterns. *Mon Weather Rev* 115:1083–1126
- Bengtsson L, Semenov V, Johannessen OM (2004) The early 20th century warming in the Arctic - a possible mechanism. *J Clim* 17:4045–4057
- Bengtsson L, Hodges KI, Roeckner E (2006) Storm tracks and climate change. *J Clim* (in press)
- Boer GJ, Yu B (2003a) Climate sensitivity and climate state. *Clim Dyn* 21: UT ISI:000185256100005
- Boer GJ, Yu B (2003b) Dynamical aspects of climate sensitivity. *Geophys Res Lett*: UT ISI:000181935000006
- Brazdil R, Pfister C, Wanner H, Storch H v, Luterbacher J (2005) Historical climatology in Europe – the state of the art. *Clim Change* 70:363–430
- Brönnimann S, Luterbacher J, Staehelin J, Svendby TM, Hansen G, Svenoe T (2004) Extreme climate of the global troposphere and stratosphere 1940–1942 related to El Niño. *Nature* 431:971–974
- Brönnimann S (2005) The global climate anomaly 1940–1942. *Weather* 60:336–342
- Collins M, Osborn TJ, Tett SFB, Briffa KR, Schweingruber FH (2002) A comparison of the variability of a climate model with paleotemperature estimates from a network of tree-ring densities. *J Clim* 15:1497–1515
- Crowley TJ (2000) Causes of climate change over the last 2000 years. *Science* 289:270–277
- Cubasch U, Voss R (2000) The influence of total solar irradiance on climate. *Space Sci Rev* 94:185–198
- Cubasch U, Hegerl GC, Voss R, Waszkewitz J, Crowley TC (1997) Simulation with an O-AGCM of the influence of variations of the solar constant on the global climate. *Clim Dyn* 13:757–767
- Fraedrich K, Müller K (1992) Climate anomalies in Europe associated with ENSO extremes, *Int J Climatol* 12:25–31
- Fröhlich C (2004) Solar irradiance variability. In: *Geophysical monograph 141: solar variability and its effect on climate*, American Geophysical Union, Washington DC, USA, Ch. 2, Solar Energy Flux Variations pp 97–110
- Fröhlich C (2006) Solar irradiance variability since 1978, revision of the PMOD composite during cycle 21. To be published by ISSI, Hallerstrasse 6, CH-3012 Bern, Switzerland
- Gerber EP, Vallis GK (2005) A stochastic model for the spatial structure of annular patterns of variability and the north atlantic oscillation. *J Clim* 18:2102–2118
- Hansen JE, Ruedy R, Mki Sato, Imhoff M, Lawrence W, Easterling D, Peterson T, Karl T (2001) A closer look at United States and global surface temperature change. *J Geophys Res* 106:23947–23963
- Hasselmann K (1976) Stochastic climate models, Part1 Theory. *Tellus* 28:273–485
- Hoskins BJ, Hodges KI (2002) New perspectives on the Northern Hemisphere winter storm tracks, *J Atmos Sci* 59:1041–1061
- Hoyt DV, Schatten KH (1993) A discussion of plausible solar irradiance variations, 1700–1992. *J Geophys Res* 98:18 895–18 906
- Hunt BG, Elliot TI (2006) Climatic Trends. *Clim Dyn* 26:567–585
- Hurrell JW, Kushnir Y, Ottensen G, Visbeck M (2003) The North Atlantic oscillation: climate significance and environmental impact., Eds. *Geophysical Monograph Series 134:279pp*
- Johannessen OM, Bengtsson L, Miles MW, Kuzmina SI, Semenov VA, Alekseev GV, Nagurnyi AP, Zakharov VF, Bobylev LP, Pettersson LH, Hasselmann K, Cattle HP (2004) Arctic climate change: observed and modeled temperature and sea ice variability. *Tellus* 56A:328–341
- Jones PD, Mann ME (2004) Climate over past millennia. *Rev of Geophys* 42: DOI: 2003RG00143
- Jungclaus J, Botzet M, Haak H, Keenlyside N, Luo JJ, Latif M, Marotzke J, Mikolajewicz U, Roeckner E (2006) Ocean circulation and tropical variability in the coupled model ECHAM5/MPI-OM. *J Clim* (in press)
- Koslowski G, Glaser R (1999) Variations in reconstructed Ice winter severity in the Western Baltic from 1501 to 1995, and their implications for the North Atlantic oscillation. *Clim Change* 41:175–191
- Lean J (2000) Evolution of the sun's spectral irradiance since the maunder minimum. *Geophys Res Lett* 27:2425–2428
- Lean J, Beer J, Bradley R (1995) Reconstruction of solar irradiance since 1610: implications for climate change. *Geophys Res Lett* 22:3195–3198
- Lin J-L, Kiladis GN, Mapes BE, Weickmann KM, Sperber KR, Lin W, Wheeler MC, Schubert SD, Del Genio A, Donner LJ, Emori S, Gueremy J-F, Hourdin F, Rasch PJ, Roeckner E, Scinocca JF (2006) Tropical intraseasonal variability in 14 IPCC AR4 climate models, part I: convective signals. *J Clim* 19:2665–2690
- Loptien U, Ruprecht E (2005) Effects of synoptic systems on the variability of the North Atlantic oscillation. *Mon Weather Rev* 133:2894–2904
- Luterbacher J, Dietrich D, Xoplaki E, Grosjean M, Wanner H (2004) European seasonal and annual temperature variability, trends and extremes since 1500. *Science* 303:1499–1503
- Manabe S, Stouffer RJ (1996) Low-frequency variability of surface air temperature in a 1000-year integration of a coupled atmosphere-ocean-land surface model. *J Clim* 9:376–393
- Mann ME, Bradley RS, Hughes MK (1999) Northern Hemisphere temperatures during the past millennium: inferences, uncertainties and limitations. *Geophys Res Lett* 26:759–762

- Marsland SJ, Haak H, Jungclaus JH, Latif M, Roeske F (2003) The Max-Planck-Institute global ocean/sea ice model with orthogonal curvilinear coordinates. *Ocean Modell* 5:91–127
- Mitchell T, Jones P (2005) An improved method of constructing a database of monthly climate observations and associated high-resolution grids. *Int J Climatol* 25:693–712
- New M, Hulme M, Jones P (2000) Representing twentieth-century space-time climate variability, part ii development of 1901–96 monthly grids of terrestrial surface climate. *J Clim* 13:2217–2238
- van Oldenborgh GJ, Philip S, Collins M (2005) El Nino in a changing climate: a multi-model study. *Ocean Sci* 1:81–95
- Rind D, Shindell D, Perlwitz J, Lerner J, Lonergan P, Lean J, McLinden C (2004) The relative importance of solar and anthropogenic forcing of climate change between the maunder minimum and the present. *J Clim* 17:906–929
- Robertson A, Overpeck J, Rind D, Mosley-Thompson E, Zielinski G, Lean J, Koch D, Penner J, Tegen I, Healy R (2001) Hypothesized climate forcing time series for the last 500 years. *J Geophys Res* 106:14783–14803
- Robock A, Free MP (1995) Ice cores as an index of global volcanism from 1850 to the present. *J Geophys Res* 100:11549–11567
- Robock A, Free MP (1996) The volcanic record in ice cores for the past 2000 years. In: Jones PD, Bradley RS, Jouzel J (eds) *Climatic variations and forcing mechanisms of the last 2000 years*. Springer, Berlin Heidelberg New York, pp. 533–546
- Roeckner E, Bäuml G, Bonaventura L, Brokopf R, Esch M, Giorgetta M, Hagemann S, Kirchner I, Kornblueh L, Manzini E, Rhodin A, Schlese U, Schulzweida U, Tompkins A (2003) The atmospheric general circulation model EC-HAM 5, PART I Model description. MPI-Report 349:127
- Roeckner E, Brokopf R, Esch M, Giorgetta M, Hagemann S, Kornblueh L, Manzini E, Schlese U, Schulzweida U (2006) Sensitivity of simulated climate to horizontal and vertical resolution. *J Clim* (in press)
- Shindell DT, Schmidt GA, Mann ME, Rind D, Waple A (2001a) Solar forcing of regional climate change during the Maunder Minimum. *Science* 294:2149–2152
- Shindell DT, Schmidt GA, Miller RL, Rind D (2001b) Northern Hemisphere winter climate response to greenhouse gas, ozone, solar and volcanic forcing. *J Geophys Res* 106:7193–7210
- Solanki SK, Usoskin IG, Kromer B, Schussler M, Beer J (2004) Unusual activity of the Sun during recent decades compared to the previous 11000 years. *Nature* 431:1084–1087
- Stendel M, Mogensen A, Christensen JH (2005) Influence of various forcings on global climate in historical times using a coupled atmosphere–ocean general circulation model. *Clim Dyn*. DOI 10.1007/s00382–005–0041–4
- von Storch H, Zorita E, Jones JM, Dimitriev Y, Gonzalez-Rouco F, Tett SFB (2004) Reconstructing past climate from noisy data. *Science* 306:679–682
- Vallis GK, Gerber EP, Kushner PJ, Cash BA (2004) A mechanism and simple dynamical model of the North Atlantic oscillation and annular modes. *J Atmos Sci* 61:264–280
- Wang Y, Lean JL, Sheeley Jr NR (2005) Modeling the Sun's magnetic field and irradiance since 1713. *Astrophys J* 625:522–538
- Wunsch C (1999) The interpretation of short climate records, with comments on the North Atlantic and Southern oscillations. *Bull Am Meteorol Soc* 80:245–255
- Xoplaki E, Luterbacher J, Paeth H, Dietrich D, Steiner N, Grosjean M, Wanner H (2005) European spring and autumn temperature variability and change of extremes over the last half millennium. *Geophys Res Lett* 32: L15713. DOI 10.1029/2005GL023424
- Yoshimori M, Stocker T, Raible CP, Renold M (2005) Externally forced and internal variability in ensemble climate simulations of the maunder minimum. *J Clim* 18:4253–4270
- Zebiak SE, Cane MA (1987) A model El Nino – Southern oscillation. *Mon Wea Rev* 115:2262–2278
- Zorita E, von Storch H, Gonzalez-Rouco FJ, Cubasch U, Luterbacher J, Legutke S, Fischer-Bruns I, Schlese U (2004) Simulation of the climate of the last five centuries. *Met Z* 13:271–289